Modeling of Damage, Permeability Changes and Pressure Responses during Excavation of the TSX Tunnel in Granitic Rock at URL, Canada

Jonny Rutqvist[1*], Lennart Börgesson[2], Masakazu Chijimatsu[3], Jan Hernelind[4], Lanru Jing[5], Akira Kobayashi[6], Son Nguyen[7]

[1] Earth Sciences Division, Lawrence Berkeley National Laboratory, MS 90-1116, Berkeley, CA 947 20, USA

[2]Clay Technology AB, Lund, Sweden

[3]Hazama Cooperation, Tokyo, Japan

[4]FEM Tech AB, Sweden

[5]Royal Institute of Technology, Stockholm, Sweden

[6]Kyoto University, Kyoto, Japan

[7]Canadian Nuclear Safety Commission, Ottawa, Canada

* Corresponding author. Tel.: +1-510-486-5432, fax.: +1-510-486-5432
E-mail address: Jrutqvist@lbl.gov (J. Rutqvist)

Abstract

This paper presents numerical modeling of excavation-induced damage, permeability changes, and fluid-pressure responses during excavation of the TSX tunnel at the underground research

laboratory (URL) in Canada. Four different numerical models were applied, using a wide range of approaches to model damage and permeability changes in the excavation disturbed zone (EDZ) around the tunnel. Using *in situ* calibration of model parameters the modeling could reproduce observed spatial distribution of damage and permeability changes around the tunnel, as a combination of disturbance induced by stress redistribution around the tunnel and by the drill-and-blast operation. The modeling showed that stress-induced permeability increase above the tunnel is a result of micro and macrofracturing under high deviatoric (shear) stress, whereas permeability increases alongside the tunnel as a result of opening of existing microfractures under decreased mean stress. The remaining observed fracturing and permeability changes around the periphery of the tunnel were attributed to damage from the drill-and-blast operation. Moreover, a reasonably good agreement was achieved between simulated and observed excavation-induced pressure responses around the TSX tunnel for 1 year following its excavation. The simulations showed that these pressure responses are caused by poroelastic effects as a result of increasing or decreasing mean stress, with corresponding contraction or expansion of the pore volume. The simulation results for pressure evolution were consistent with previous studies, indicating that the observed pressure responses could be captured in a Biot model using a relatively low Biot-Willis' coefficient, $\alpha \approx 0.2$, a porosity of $n \approx 0.007$, and a relatively low permeability of $k \approx 2\times10^{-22}$ m^2, which is consistent with the very tight, unfractured granite at the site.

Keywords: coupled processes, excavation disturbed zone, damage, permeability, TSX

1 Introduction

The performance assessment of geological disposal for spent nuclear fuel requires consideration of coupled thermal, hydrological, and mechanical (THM) processes, especially in the rock near disposal tunnels where coupled processes are at their highest intensity. In particular, coupled processes in the excavation disturbed zone (EDZ) and its potential impact on the repository performance needs to be understood (Bäckblom and Martin 1999; Rutqvist and Stephansson 2003; Tsang and others 2005). Several field studies have shown that the EDZ includes a damaged zone of induced rock failure and fracturing, stemming from excavation processes, as well as a zone with altered stress distribution around the tunnels. For mechanical excavation (using no blasting) in a moderate-stress environment, the damage zone may be limited to a few centimeters thickness, where a limited change in porosity and permeability may take place. When drill-and-blast is used for excavation, the damage zone is more extensive, and therefore increased permeability is likely, especially in the tunnel floor, where the permeability can increase by two to three orders of magnitude (Bäckblom and Martin 1999). The EDZ has the potential to affect the short- and long-term structural stability of a repository, as well as the effectiveness of the rock mass as a contaminant transport barrier.

This paper presents numerical analyses of a tunnel excavation in granitic rock, with the purpose of validating and, if necessary, calibrating the hydraulic and mechanical rock properties to be used for modeling of a hypothetical nuclear waste repository in the same type of rock. The study was conducted as part of the DECOVALEX-THMC project (2004-2007), Task A, related to assessing the implications of coupled THM processes in the near field of a typical repository, with special emphasis on the impact of rock damage and bentonite behavior on long-term repository performance (Nguyen and others 2008a). A major part of this task was development

and calibration of material models for Lac du Bonnet granite (Nguyen and others 2008b) and the MX-80 bentonite (Chijimatsu and others 2008a), using a variety of laboratory and field experiments. This paper focuses on validating and calibrating coupled hydraulic and geomechanical material models of Lac du Bonnet granite, using field observations and measurements made during excavation of a test tunnel associated with the Tunnel Sealing Experiment (TSX) at the Underground Research Laboratory (URL) in Canada. Specifically, measurements of excavation-induced damage, permeability changes, and fluid pressure responses were used for model validation and calibration. Four research teams simulated the excavation of the tunnel using a wide range of approaches for modeling damage and permeability changes in the EDZ (Table 1). This paper first summarizes relevant field observations at the TSX tunnel and briefly describes the models applied. The next two subsections present modeling of excavation-induced damage and permeability changes, as well as modeling of excavation-induced pressure changes. We conclude by describing the causes of excavation-induced permeability changes as a combination of stress redistribution around the tunnel and drill-and-blast damage. Finally, we provide some perspective on how these results can be used in predicting the evolution of the EDZ at a spent nuclear fuel repository.

2 Relevant field observations at the TSX tunnel

The TSX tunnel (Room 425) excavated at a depth of 420 m is one of a series of experimental tunnels at URL that have been studied with respect to the evolution of the EDZ around tunnels in granitic rock (Martino and Chandler, 2004). To minimize the EDZ, the TSX tunnel was excavated using smooth drill-and-blast techniques in an elliptical cross section of 3.5 m high,

4.375 m wide (with a horizontal to vertical aspect ratio of 1.25). At the site, the principal stresses are estimated to 60 MPa (maximum stress), 45 MPa (intermediate stress) and 11 MPa (minimum stress), with the maximum principal stress being parallel with the tunnel axis and the minimum principal stress being subvertical. During excavation, the occurrence and location of microseismic events were monitored. After excavation, the resulting EDZ was characterized by a variety of methods, including the microvelocity probe (MVP) method for measuring changes in sonic velocities, and the SEPPI method for measuring changes in permeability (Figure 1). The SEPPI probe provided a measure of the rock transmissivity for small intervals along a series of boreholes penetrating the EDZ. Moreover, for a period of 1 year after excavation, pore pressure was monitored in the rock at various distances from the tunnel.

Results from each EDZ characterization method indicated that a damage zone of a certain thickness exists around the TSX tunnel. Borehole measurements indicated the existence of an inner damage zone within 0.3 m from the tunnel wall, delineated from the outer portion of the EDZ by a more rapid decrease in velocity and more rapid increase in transmissivity (Figure 1). The outer damage zone, which was detected by all instruments used, displayed a more gradual change in velocity and hydraulic transmissivity that ultimately returned to background levels with increased downhole distance. Beyond the outer damage zone is the excavation disturbed zone. Borehole camera surveys showed an increased degree of macroscopic damage (visible fractures) in the inner damage zone area. The highest hydraulic transmissivities were generally recorded in the regions where the borehole camera detected the majority of the fracturing along the borehole walls (Martino and Chandler, 2004).

The cause of the visible (macroscopic) fracturing around the periphery of the tunnel could be a combination of damage caused by the excavation process (e.g. dynamic forces during drilling and blasting) and damage caused by stress concentrations around the tunnel opening. That at least some of the observed fracturing is caused by the excavation process is indicated by observations of similar extent of the damage zone around a tunnel (BDA tunnel) excavated with the same drill-and-blast method at 240 m depth, where the *in situ* stress magnitudes are low enough that stress-induced damage does not generally occur around the tunnels (Martino and Chandler, 2004). However, Figure 1 indicates a notch-like extension of the inner damage zone detected by the SEPPI measurements at the top and bottom of the tunnel. This notch may be related to high stress concentrations that could create new fractures or extend and open fractures created by the drill-and-blast operation. Moreover, monitoring of microseismic events shows clusters surrounding the notches at the top and bottom to the tunnel cross section (Martino and Chandler, 2004). On the other hand, no extensive fall-out of rock was recorded. This observation is consistent with other studies at the URL, because the maximum compressive stress at the top of the TSX tunnel is estimated to be about 100 MPa—slightly lower than the *in situ* compressive strength, which has been estimated to be about 120 MPa at URL (Martin, 2005). For example, at the URL's mine-by experiment, the maximum compressive stress exceeded 120 MPa, and substantial spalling and notch-shaped fall-out of rock were recorded at the top of the tunnel (Martin and others 1997; Martin 2005).

The excavation of the TSX tunnel resulted in changes in fluid pressure in the surrounding rock (Figure 2). In general, the initial fluid pressure before excavation of the TSX tunnel was about 3 MPa, lower than the theoretic hydrostatic pressure at 420 m depth as a result of a pressure sink

caused by nearby open excavations. During the excavation of the TSX tunnel, the pressure changed rapidly, increasing at locations above the tunnel and decreasing at locations alongside the tunnel. This initial pressure pulse was attributed to undrained poroelastic response as a result of excavation-induced volumetric contraction or expansion of the low-permeability rock surrounding the TSX tunnel. After this initial pressure pulse, Figure 2 shows that the fluid pressure slowly decays as fluid pressure tends to equilibrate with the ambient pressure conditions. However, several years after the excavation, fluid pressure was still elevated above the TSX tunnel.

3 TSX model setup

All the research teams discretized the problem into a two-dimensional vertical cross section. This cross section was symmetrical, so only one half of the tunnel had to be discretized. The initial stresses were set to σ_1 = 60 MPa, σ_2 = 45 MPa, σ_3 = 11 MPa, according to the best estimate of the *in situ* stress field at TSX. The initial fluid pressure was set to 3 MPa, whereas after excavation, the fluid pressure at the tunnel wall was set to atmospheric.

A consistent set of basic mechanical and hydraulic material parameters, representing the Lac du Bonnet granite and the Canadian Shield rock properties, were provided to the research teams. This included Young's modulus of E = 60 GPa, Poisson's ratio of ν = 0.2, Biot-Willis' effective stress coefficient of α = 0.2, permeability of $k = 7.0\times10^{-19}$ m^2, as well a recommended rock-mass strength parameters for the Hoek and Brown failure criterion (Nguyen and Jing, 2008). For determining the safety factor of excavations in Lac du Bonnet granite, Baumgartner and others (1996) recommended the use of the Hoek and Brown criterion

$$\sigma_1' = \sigma_3' + \sigma_{ci}\left(m\frac{\sigma_3'}{\sigma_{ci}} + s \right)^a \quad (1)$$

with the following parameters: σ_{ci} = 100 MPa, s = 1, m = 16.6, and a = 0.5. These rock mass strength parameters were recommended as to reflect the *in situ* rock-mass strength, including *in situ* uniaxial compressive strength that is roughly half of the instantaneous uniaxial compressive strength determined from testing of core samples.

The given set of parameters were those recommended for the analysis of the hypothetical nuclear waste repository (Nguyen and others 2008a) and were to be used as a set of starting parameters in the TSX tunnel analysis. It was recognized early on though, that the permeability of 7.0×10^{-19} m^2 recommended for sparsely fractured rock of the Canadian Shield was too high for the virtually unfractured (intact) rock surrounding the TSX tunnel. For example, the estimates from the SEPPI probe indicate permeability on the order of 1×10^{-20} m^2 (Martino and Chandler, 2004) or 1×10^{-21} m^2 (Souley and others, 2001), but a value as low as 1×10^{-23} m^2 has been calibrated in an earlier modeling study of poroelastic responses during a heating experiment at TSX (Gou and Dixon 2006). Moreover, the apparent low value of Biot-Willis' effective stress parameter (α = 0.2) was also determined by model calibration (Gou and Dixon, 2006), whereas laboratory tests on core samples by Lau and Chandler (2004) indicate a much higher value of α = 0.73. Accordingly, an important task for this study was to validate or refute these recommended parameters and perform model calibration of the parameters required for the respective models.

The original plan was to develop, test, and calibrate damage models against laboratory experiments, following the approach used in an earlier study by Souley and others (2001). However, it was found that the model parameters derived from the short-term cyclic triaxial

laboratory tests were not representative of *in situ* behavior, but had to be calibrated to represent the lower *in situ* strength at the TSX tunnel. The continuum damage model used by the JAEA team and the Drucker-Prager model used by the CLAY-SKB team are described in detail in the accompanying paper by Nguyen and others (2008b). In contrast, here we focus on how the respective models were applied to simulate damage and permeability changes, and how the input parameters to the respective models had to be adjusted to represent the *in situ* behavior at the TSX tunnel.

4 Modeling of excavation-induced damage and permeability change

With the assumed stress field, the maximum principal compressive stress is about 100 MPa at the top of the tunnel, whereas a slight tensile stress occurs at the side of the tunnel. Thus, for macroscopic failure to occur at the top of the tunnel, the *in situ* compressive strength should be less than about 100 MPa. Moreover, the high stress concentration at the top of the tunnel leads to a volumetric contraction in that area, whereas a general unloading leads to volumetric expansion at the side of the tunnel. This fact is important for explaining the difference in the excavation induced damage, permeability, and pressure responses around the tunnel. In the next four subsections, the model calibration and results for induced damage and permeability derived by each of the four research teams are described in more detail.

4.1 The CNSC model calibration of damage and permeability change

The CNSC research team evaluated damage using the MSDPu criterion proposed by Aubertin and others (2000) and Li and others (2005). The input parameters for the MSDPu criterion were inferred from laboratory triaxial test and field observations. In particular, the input parameters defining the MSDPu yield function were derived by fitting it to the recommended Hoek and

Brown yield function. The resulting strength parameters include a uniaxial compressive strength of 110 MPa, and a uniaxial tensile strength of 5 MPa (Nguyen and Jing, 2008). Using these parameters, the calculated extent and shape of the yield zone (the zone in which the stress state has exceeded the rock strength) is similar to the so-called inner damage zone observed in the field (compare Figure 3a with Figure 1).

To simulate the increased permeability around the tunnel and in the EDZ, using an approach similar to that used by Mahyari and Selvadurai (1998) and Shirazi and Selvadurai (2005), the CNSC research team assumed that permeability, k, varied with equivalent deviatoric strain, according to

$$k = k_i \exp(\beta \varepsilon_d) \tag{2}$$

where k_i is the initial (pre-excavation) permeability and β is a fitting constant, and ε_d is equivalent deviatoric strain defined as

$$\varepsilon_d = \frac{2}{\sqrt{6}} \sqrt{(\varepsilon_1 - \varepsilon_2)^2 + (\varepsilon_2 - \varepsilon_3)^2 + (\varepsilon_3 - \varepsilon_1)^2} \tag{3}$$

where ε_1, ε_2, and ε_3 are principal strains.

By adopting $k_i = 0.5 \times 10^{-21}$ m^2 and $\beta = 7000$, the CNSC research team obtained a reasonable good match between simulated and measured values of permeability increases above the tunnel (Figure 3b). The calculated permeability profile indicates progressively increasing permeability towards the tunnel wall as a result of the increasing deviatoric strain. In the damaged (yield) zone extending about 0.2 m into the rock above the tunnel, the permeability increase is amplified by the additional plastic deviatoric strain. However, this model may not predict any significant

permeability increase near the side wall of the tunnel, where deviatoric stress and strain are small.

4.2 The JAEA model calibration of damage and permeability change

The JAEA research team applied a classical continuum damage model (Lemaitre, 1992) to simulate the damage evolution and its impact on permeability (Murakami and Kamiya, 1997). The JAEA first simulated laboratory experiments to determine six damage parameters needed for the damage model—see Chijimatsu and others (2008b) and Nguyen and others (2008b). However, when simulating the TSX experiment, some of the damage variables had to be significantly lowered to match field observations (Chijimatsu and others 2008b). This included lowering a parameter called the initial damage potential, B_0, as well as another parameter, K_v, that affects the rate of expansive strain with damage. Using such lowering of the damage parameters, the JEAE research team achieved a better agreement between the simulated and observed damage pattern. Specifically, if the damage parameters determined from the small-scale laboratory experiments were used as input, no damage occurred. When the parameters where lowered, damage occurred around the entire periphery of the tunnel, including at the top of the tunnel, where the failure is caused by high compressive stresses (Compare Figure 4a with Figure 1).

Changes in permeability around the tunnel were estimated by first calculating the evolution of porosity as a function of total volumetric strain, ε_v, which is the sum of the elastic volumetric strain and the isotropic expansive strain caused by damage, according to:

$$\varepsilon_v = \varepsilon_v^{elastic} + \varepsilon_v^{damage} \tag{4}$$

According to the damage model, the isotropic expansive strain is proportional to the equivalent conjugate damage force, which in turn depends on the damage variable, *D*, and the damage parameters B_0 and K_v (Chijimatsu and others 2008b: Nguyen and others 2008b). The permeability, *k*, (unit of m^2) was related to porosity, *n*, using the following empirical permeability-versus-porosity function:

$$k = 2.186 \times 10^{-10} n^3 - 5.8155 \times 10^{-18} \quad (5)$$

This permeability-versus-porosity function has been derived using grantitic rock samples from the Canadian Shield (Katsube and Kamineni, 1983), with permeability ranging between 10^{-19} m^2 and 10^{-17} m^2. The function in Equation (5) and its match with the experimental data is presented in Chijimatsu and others (2005), and was also applied in Millard and others (2005) for modeling of permeability changes around a hypothetical nuclear waste repository in the same type of rock. The JAEA assumed the initial permeability to be 7.0×10^{-19} m^2, which according to Equation (5) corresponds to an initial porosity 0.0031. Permeability on the order of 7.0×10^{-19} m^2 is representative of an equivalent permeability for sparsely fractured rock, intended to be used as a base case for modeling of a hypothetical repository in Nguyen and others (2008a). However, this value is several orders of magnitude higher than the initial (pre-excavation) permeability measured for the tight intact rock surrounding the TSX experiments.

The simulated post-excavation permeability distribution is shown in Figure 4b. The simulated result shows a two-order-of-magnitude increase at the side of the tunnel, which is comparable to the observed changes in transmissivity in Figure 1. The simulated results indicated smaller changes in permeability above the tunnel. In that region, the expansive volumetric strain by

damage may be offset by a contractive elastic volumetric strain caused by the strongly increased mean stress.

4.3 The CLAY-SKB model calibration of damage

The CLAY-SKB research team applied a Drucker-Prager plasticity model to simulate damage around the TSX tunnel. The Drucker-Prager model was also successfully applied to model the cyclic stress-strain behavior of small scale laboratory experiments (See Börgesson and Hernelind 2008; Nguyen and others 2008b). However, similarly to the results of CNSC and JAEA, the elasto-plastic material parameters derived from the small-scale laboratory experiment could not be used to reproduce the observed damage at the TSX tunnel. The possibility of reducing both cohesion and friction angle were investigated: Lowering the cohesion to zero resulted in small compressive failure at the side of the tunnel, whereas lowering the friction angle to zero resulted in compressive failure at the top of the tunnel (Figure 5). Lowering the friction angle to zero is consistent with a so-called spalling criterion according to Martin (2005), which tends to better predict the shape of spalled zone around tunnels. However, the cohesion should then be chosen to represent the *in situ* compressive strength.

4.4 The LBNL-SKI model calibration of damage and permeability change

The approach adopted by the LBNL-SKI team was to derive a simplified but practical model that could be implemented in the ROCMAS code, but could yet capture reasonably well the observed damage and permeability changes at the URL field experiments. Parameters for a Mohr-Coulomb criterion were fitted to the recommended Hoek-Brown failure envelope to derive an equivalent cohesion of C = 18.7 MPa and an equivalent friction angle of ϕ = 49°. Using such

parameters, the LBNL-SKI simulation resulted in a limited yielding at the crown of the tunnel, which is in agreement with observed increased macroscopic fracturing at the top of the TSX tunnel. This area also coincides with the region where most microseismic events were clustered. Similarly to previous studies at the URL Mine-by experiments (Martin, 2005), the LBNL team found that the region of microseismic events is the area of highest shear stress.

The permeability around the tunnel was simulated using an empirical stress-versus-permeability relationship in which permeability is a function of effective mean stress, σ'_m, and deviatoric stress, σ_d, according to:

$$k = [k_r + \Delta k_{\max} \exp(\beta_1 \sigma'_m)] \cdot \exp(\gamma \Delta \sigma_d) \tag{6}$$

where k_r is residual (or irreducible) permeability at high compressive mean stress, and Δk_{max}, β_1 and γ are fitting constants. The effective mean stress, σ'_m, formally the mean of normal stresses and the deviatoric stress, σ_d, are defined as

$$\sigma'_m = \frac{1}{3}(\sigma_1 + \sigma_2 + \sigma_3) - P \tag{7}$$

$$\sigma_d = \frac{1}{\sqrt{2}} \sqrt{(\sigma_1 - \sigma_2)^2 + (\sigma_2 - \sigma_3)^2 + (\sigma_1 - \sigma_3)^2} \tag{8}$$

where σ_1, σ_2 and σ_3 are the principal stresses with compressive stress positive.

Figure 6 compares simulated and measured permeability changes for $\beta_1 = 4 \cdot 10^{-7}$ Pa^{-1}, $k_r = 2 \cdot 10^{-21}$ m^2, $\Delta k_{max} = 8 \cdot 10^{-17}$ m^2, $\gamma = 3 \cdot 10^{-7}$ Pa^{-1}, and the critical deviatoric stress for onset of shear induced permeability is set to 55 MPa. The 55 MPa critical deviatoric stress roughly coincides with the extent of the observed cluster of microseismic events at the top of the tunnel (see microseismic clusters in Martino and Chandler 2004). Thus, the 55 MPa critical stress is an important

parameter for matching the observed permeability changes at the top of the tunnel. The 55 MPa deviatoric stress corresponds to about 0.3 of the instantaneous uniaxial compressive stress of small-scale core samples, which is consistent with the stress level at which crack-initiation has been observed in studies of Lac du Bonnet granitic samples (Martin and Chandler, 1994). Thus, this indicates that at least part of the observed permeability increase above the tunnel are caused by microfracturing under high compression, whereas permeability increases off the side of the tunnel is caused by opening of existing microfractures as a result of decreased mean stress. However, the comparison of the simulated and measured permeability changes around the tunnel indicates that the model captures the permeability increase caused by reduction in mean stress at the side of the tunnel reasonably well, whereas the permeability increases at the top of the tunnel are partly underestimated (Figure 6). It is possible that the several-orders-of-magnitude increase in permeability measured at the top of the tunnel is caused by macroscopic fracturing that was indeed observed in the boreholes. The macrofracturing implies that a simple relationship between mean and deviatoric stress, as defined in Equation (6) may not longer be valid. Instead, the permeability may be governed by fracture permeability as a function of stress normal to the fracture planes.

Figure 7 presents contours of simulated permeability change around the tunnel. Figure 7a presents the stress induced permeability changes using Equation (6). To obtain a good match with field observations in Figure 1, the LBNL-SKI team manually added additional damage induced permeability caused by drill-and-blast operations for a zone extending about 0.3 m all around the tunnel (Figure 7b). The resulting calibrated stress-versus-permeability function according to Equation (6) is presented in Figure 8 at various confining stresses. The curves in

Figure 8 bear some resemblance to laboratory data on permeability versus deviatoric stress presented in Shao and others (2005). However, the laboratory data in Shao and others (2005) were from a short-term experiment, which can explain the higher deviatoric stress required to observe substantial dilatant permeability increase.

5 Results of excavation-induced pressure changes

Two teams, CNSC and LBNL-SKI modeled stress-induced changes in pore pressure during excavation of the TSX tunnel. Both teams simulated the excavation of the TSX tunnel by gradually removing the internal fluid pressure and stresses within the tunnel over one month. The modeling explains the observed pressure responses as an initial stress-induced pressure pulse when an excavation front passes parallel to the monitoring points, followed by a year-long diffusion-induced pressure recovery. These early-time pressure changes are caused by pore-volume changes that are in turn caused by changes in mean stress and volumetric strain around the excavation (Figure 9a). Above the tunnel, the mean stress increases, causing contractive volumetric strain and reduced pore-volume, which in turn leads to a transient increase in fluid pressure. Alongside the tunnel, the mean stress decreases, causing expansion of the pore-volume that leads to a decrease in fluid pressure. After one year, much of the stress-induced pressure change has diffused by fluid flow (Figure 9b).

Parameter studies showed that the excavation-induced evolution of fluid pressure depends on the following material parameters:

1) Permeability
2) Biot's parameters α and M

3) Bulk modulus, K

The bulk modulus is given from the Young's modulus and Poisson's ratio used above and is roughly 33 MPa for the undisturbed rock. Biot-Willis' constant α is defined as

$$\alpha = 1 - \frac{K}{K_s} \tag{9}$$

where K_s is the bulk modulus of the grains (Wang 2000). As a starting point, a Biot-Willis' constant of α = 0.2 was suggested. Moreover, Biot's modulus *M*, can be estimated using the following relationship (Detournay and Cheng 1993):

$$\frac{1}{M} = \frac{n}{K_f} + \frac{\alpha - n}{K_s} \tag{10}$$

where *n* is porosity and K_f is the fluid bulk modulus.

The parameter study showed that the poroelastic parameters (Biot's parameters α and *M*, and the bulk modulus *K*) strongly affect the magnitude of the initial pressure pulse, whereas the permeability mostly affects the subsequent pressure recovery. The effect of α, *M*, and *K* on the pressure pulse can be explained by the Skempton's coefficient, *B*, defined to be the ratio of the induced pore pressure to the change in applied stress for undrained conditions, which can be related to the above parameters as (Detournay and Cheng, 1993):

$$B = \frac{M\alpha}{K + \alpha^2 M} \tag{11}$$

The CNSC research team used a permeability of 5×10^{-21} m^2, as estimated from SEPPI measurements, and which the CNSC team also previously used for their analysis of excavation-induced permeability changes. However, it was found that pressure dissipation would be too fast with such permeability and would not match the very slow pressure dissipation observed in the field.

Figure 10 presents the results from the LBNL-SKI research team, with a detailed comparison of simulated and measured pressure responses at the four measurement points closest to the TSX tunnel. Using $\alpha = 0.2$, $M = 130$ GPa, $K = 60$ MPa, and a very low permeability of $k = 2\times10^{-22}$ m^2 (simulation a) the calculated pressure response in HTG1-4 closely matches the measured one. However, using this set of data, the pressure pulse in HTG1-5 would be overestimated. To obtain a good match in HTG1-5 the parameters were adjusted to $\alpha = 0.17$, $M = 140$ GPa, $K = 60$ MPa, and $k = 3\times10^{-22}$ m^2 (Simulation b). This slight adjustment of the parameters may not be unrealistic, considering natural heterogeneities and the fact that stresses increase to a much higher level at HTG1-5 than at HTG1-4. In fact, the poroelastic parameters K, α, M are likely to be stress dependent; a lower α and higher modulus are indeed expected at a higher stress. Using the two sets of parameters (simulation a and b), a porosity of $n \approx 0.007$ can be estimated from Equation (10).

The results alongside the tunnel (HGT2-3 and HGT2-4) indicate similar trends between simulated and measured responses, except for the measured trend of increasing pressure in HGT2-3. Such an upward trend in fluid pressure was observed in several measurement intervals (not shown in Figure 10) located away from the TSX tunnel, and seem to reflect a general pressure trend in the area, possibly affected by other nearby activities.

6 Concluding remarks

In this study, a wide range of models and approaches were applied to investigate excavation-induced evolution of damage, permeability changes, and fluid pressure around the TSX tunnel at URL, Canada.

To match the observed damage and permeability increases around the tunnel, the model parameters had to be calibrated using lower strength parameters than those obtained from short-term laboratory experiments on the same type of rock. Using a lowering for the rock strength parameters, e.g. a uniaxial compressive strength of 50 to 60% of the laboratory short-term strength, the models predicts limited damage and yielding at the crown (top) of the tunnel as a result of high compressive and deviatoric stress (up to 100 MPa) in that area. Some models also predict damage at the springline (side) of the tunnel. The limited yielding at the top of the tunnel is consistent with an increase in macrofracturing and microseismic events observed in that area.

The observed permeability increases around the tunnel could be explained by a decrease in mean effective stress where permeability increased at the side of the tunnel, or by high deviatoric (shear) stress and strain at the top of the tunnel. The increased permeability at the top of the tunnel is consistent with a zone of observed microseismic events, indicating that these permeability changes are caused by microfracturing, and macrofracturing, which is also consistent with the calculated zone of yielding close to the tunnel wall in this area. In addition to the stress-induced damage and permeability changes, effects of the drill-and-blast operation would have to be added to explain the observed damage and permeability enhancement around the entire periphery of the tunnel.

The observed transient pressure evolution could be reasonably well captured and explained by coupled hydraulic and mechanical responses, according to Biot's theory. In general, to match the observed pressure evolution, the basic rock permeability had to be lowered by more than one order of magnitude compared to the values estimated from borehole probe measurements. On the other hand, the best-match permeability of about $k \approx 2\times10^{-22}$ m^2 is consistent with intact rock permeability of low-permeability granite. Such a low permeability and an apparent low Biot-Willis' coefficient ($\alpha \approx 0.2$) is also consistent with earlier *in situ* estimates at the tunnel site (Gou and Dixon, 2006).

This study demonstrates the usefulness and the importance of *in situ* experiments for model calibration and validation. The important differences and relations between laboratory and *in situ* strength properties were highlighted. However, with proper consideration, the model simulations conducted in this study could be used to capture and explain the observed coupled hydraulic and mechanical responses at the TSX experiment. In particular, the observed stress-induced permeability changes in the EDZ could be explained and captured in the modeling. This provides confidence in the models, which can then be used to predict how permeability will evolve after emplacement of heat-releasing waste. Such processes and their implications for the performance of a nuclear waste repository are studied in the accompanying paper by Nguyen and others (2008a) in the same type of rock, as well as in Rutqvist and others (2008) for repository in a fractured rock mass.

Acknowledgments

Funding to the LBNL research team and the first author was provided by the Swedish Nuclear Waste Power Inspectorate (SKI), through U.S. DOE–LBNL Contract No. DE-AC02-05CH11231. Funds for modeling work by other research teams were provided by the Japanese Atomic Energy Agency (JAEA), the Canadian Nuclear Safety Commission (CNSC), and the Swedish Nuclear Fuel and Waste Management Company (SKB).

It is emphasized that the views expressed in this paper are solely those of the authors and cannot necessarily be taken to represent the views of any of the organizations listed above.

References

Alonso EE and others (2005) The FEBEX bechmark test. Case definition and comparison of modelling approaches. Int J Rock Mech Min Sci 42:611–638.

Aubertin M, Li L, Simon R (2000) A multiaxial stress criterion for short- and long-term strength of isotropic rock media. Int. J Rock Mech Min Sci 37:1169–1193.

Baumgartner P and others (1996) Engineering for a disposal facility using the in-room emplacement method. AECL report 11595, COG-96-223. Whiteshell Laboratories, Pinawa, Manitoba, Canada.

Bäckblom G, Martin CD (1999) Recent experiments in hard rock to study the excavation response: Implication of the performance of a nuclear waste geological repository. Tunneling and Underground Space Technology 14:377–394.

Börgesson L, Hernelind J (2008) Development and calibration of THM models of the rock and the buffer. In Nguyen TS and Jing L, editors, DECOVALEX-THMC project, Task A, Influence of near-field coupled THM phenomena on the perfomrance of a spent nuclear fuel repository. Report of Task A2. Swedish Nuclear Power Inspectorate, SKI Technical Report, Stockholm, Sweden.

Börgesson L, Chijimatsu M, Nguyen TS, Rutqvist J, Jing L (2001) Thermo-hydro-mechanical characterization of a bentonite-based buffer material by laboratory tests and numerical back analyses. Int J Rock Mech Min Sci 38:105–127.

Chandler NA, Cournut D, Dixon C. Fairhurst C, Hansen F, Gray M, Hara K, Ishijima Y, Kozak E, Martino J, Masumoto K, McCrank G, Sugita Y, Thompson P, Tillerson J, Vignal B (2002) The five-year report on the tunnel sealing experiment: an international project of

AECL, JNC, ANDARA and WIPP, AECL Whiteshell Laboratories, Pinawa, Manitoba, AECL-12127.

Chijimatsu M and others (2008a) Model development and calibration of the coupled thermal, hydraulic and mechanical phenomena on bentonite. Environmental Geology (this issue).

Chijimatsu M, Tsukada Y, Kobayashi A, Fujisaki K, Fujita T (2008b) JAEA team results for subtask A-2: model development and calibration of rock mass and bentonite. In Nguyen TS and Jing L, editors, DECOVALEX-THMC project, Task A, Influence of near-field coupled THM phenomena on the perfomrance of a spent nuclear fuel repository. Report of Task A2. Swedish Nuclear Power Inspectorate, Stockholm, Sweden.

Chijimatsu M, Nguyen TS, Jing L, de Jonge J, Kohlmeier M, Millard A, Rejeb A, Rutqvist J, Souley M, Sugita Y (2005) Numerical study of the THM effects on the near-field safety of a hypothetical nuclear waste repository – BMT1 of the DECOVALEX III project. Part 1: Conceptualization and characterization of the problems and summary of results. Int J Rock Mech Min Sci 42:720–730.

Detournay E, Cheng AH-D (1993) Fundamentals of poroelasticity. In Hudson JA, editor, comprehensive rock engineering: principles, practice and projects, vol 2, pp. 113-171, Pergamon Press, Oxford, UK.

Gou R, Dixon D (2006) Thermohydromechanical simulations of the natural cooling stage of the Tunnel Sealing Experiment. Engineering Geology 85: 313–331.

Katsube TJ, Kamineni DC (1983) Effect of alteration on pore structure of chrystalline rocks;core samples from Atikokan, Ontario. Can Mineral 21: 637–646.

Kobayashi A, Fujita T, Chijimatsu M (2001) Continuous approach for coupled mechanical and hydraulic behavior of fractured rock mass during hypothetical shaft sinking at Sellafield, UK. Int J Rock Mech Min Sci 38: 45–57.

Lau JSO, Chandler NA (2004) Innovative laboratory testing. Int J Rock Mech Min Sci 41: 1427–1445.

Lemaitre J (1992) A course on damage mechanics, Berlin: Springer-Verlag.

Li L, Aubertin M, Simon R, Bussière B (2005) Formation and application of a general inelastic locus for geomaterial with variable porosity. Canadian Geotechnical Journal 42: 601–642.

Mahyari AT, Selvadurai APS (1998) Enhanced consolidation in brittle geomaterials susceptible to damage, Mechanics of Coh-Frict Mat 3:291–303.

Martin CD, Read RS, Martino JB (1997) Observations of brittle failure around a circular test tunnel. Int J Rock Mech Min Sci 34: 1065–1073.

Martin D (2005) Preliminary assessment of potential underground stability (wedge and spalling) at Forsmark, Simpevarp and Laxemar sites. SKB report R-05-71.

Martin CD, Chandler NA (1994) The progressive fracture of Lac du Bonnet Granite. Int J Rock Mech Min Sci & Geomech Abstr 31: 643–659.

Martino JB, Chandler NA (2004) Excavation-induced studies at the Underground Research Laboratory. Int J Rock Mech Min Sci 41: 1413–1426.

Millard A, Rejeb A, Chijimatsu M, Jing L, de Jonge J, Kohlmeier M, Nguyen TS, Rutqvist J, Souley M, Sugita Y (2005) Numerical study of the THM effects on the near-field safety of a hypothetical nuclear waste repository – BMT1 of the DECOVALEX III project. Part 2: Effects of THM coupling in continuous and homogeneous rock. Int J Rock Mech Min Sci 42:731–744.

Min KB, Rutqvist J, Tsang C-F Jing L (2005) Thermally induced mechanical and permeability changes around a nuclear waste repository – a far-field study based on equivalent properties determined by a discrete approach. Int J Rock Mech Min Sci 42**:** 765–780.

Murakami S, Kamiya K (1997) Constitutive damage evolution equation for elastic-brittle material based on irreversible thermodynamics. In J Mech Sci 39:473–486.

Nguyen TS, Börgesson L, Chijimatsu M, Rutqvist J, Fujita T, Hernelin J, Kobayashi A, Onishi Y, Tanaka M, Jing L (2001) Hydro-mechanical response of a fractured rock mass to excavation of a test pit – The Kamaishi Mine Experiment in Japan. Int J Rock Mech Min Sci 38:79–94.

Nguyen TS and others (2008a) A case study on the influence of THM coupling on the near field safety of a spent fuel repository in sparsely fractured granite. Environmental Geology (this issue).

Nguyen TS and others (2008b) Damage of granite in cyclic triaxial tests: experimental observations and model development. Environmental Geology (this issue).

Nguyen TS and Jing L (2008) SKI report DECOVALEX-THMC project, Task A, Influence of near-field coupled THM phenomena on the perfomrance of a spent nuclear fuel repository. Report of Task A2. Swedish Nuclear Power Inspectorate, Stockholm, Sweden.

Nguyen TS, Selvadurai APS (1995) Coupled thermal-mechanical-hydrological behaviour of sparsely fractured rock: implications for nuclear fuel waste disposal, Int J Rock Mech Min Sci & Geomech Abstr 32:465–480.

Nguyen TS, Börgesson L, Chijimatsu M, Rutqvist J, Fujita T, Hernelin J, Kobayashi A, Onishi Y, Tanaka M, Jing L (2001) Hydro-mechanical response of a fractured rock mass to excavation of a test pit – The Kamaishi Mine Experiment in Japan. Int J Rock Mech Min Sci 38:79–94.

Noorishad J, Tsang C-F (1996) ROCMAS-simulator: A Thermohydromechanical Computer Code. In Stephansson, O., Jing, L., and Tsang, C.-F. editors. *Coupled Thermo-hydro-mechanical Processes of Fractured Media*. Developments in Geotechnical Engineering, Elsevier, 79, pp. 551–558.

Ohnishi Y, Shibata H, Kobayashi A (1987) Development of finite element code for the analysis of coupled thermo-hydro-mechanical behavior of a saturated-unsaturated medium. In C.-F. Tsang, editor, Coupled Processes Associated with Nuclear Waste Repositories, Academic Press, 551–557.

Ohnishi Y, Kobayashi A (1996) THAMES. In O. Stephansson, L. Jing, and C.-F. Tsang, editors, Coupled Thermo-hydro-mechanical Processes of Fractured Media, Developments in Geotechnical Engineering, Elsevier, 79:545–549.

Rutqvist J, Stephansson O (2003) The role of hydromechanical coupling in fractured rock engineering. Hydrogeology Journal 11:7–40.

Rutqvist J, Börgesson L, Chijimatsu M, Kobayashi A, Nguyen TS, Jing L, Noorishad J, Tsang C-F (2001a) Thermohydromechanics of partially saturated geological media – Governing equations and formulation of four finite element models. Int J Rock Mech Min Sci 38:105-127.

Rutqvist J, Börgesson L, Chijimatsu M, Nguyen TS, Jing L, Noorishad J, Tsang CF (2001b) Coupled thermo-hydro-mechanical analysis of a heater test in fractured rock and bentonite at Kamaishi Mine – Comparison of field results to predictions of four finite element codes. Int J Rock Mech Min Sci 38:129–142.

Rutqvist J, Chijimatsu M, Jing L, de Jonge J, Kohlmeier M, Millard A, Nguyen TS, Rejeb A, Souley M, Sugita Y, Tsang CF (2005) Numerical study of the THM effects on the near-field safety of a hypothetical nuclear waste repository – BMT1 of the DECOVALEX III project. Part 3: Effects of THM coupling in fractured rock. Int J Rock Mech Min Sci 42:745–755.

Rutqvist J, Bäckström A, Chijimatsu M, Feng X-T, Pan P-Z, Hudson J, Jing L, Kobayashi A, Koyama T, Lee H-S, Huang X-H, Rinne M, Shen B (2008) A Benchmark Simulation Study of the Long-term EDZ Evolution of Geological Nuclear Waste Repositories. Environmental Geology (this issue).

Shao JF, Zhou H, Chau KT (2005) Coupling between anisotropic damage and permeability variation in brittle rocks. Int J Numer Anal Meth Geomech, 29:1231–1247.

Shirazi A, Selvadurai APS (2005) Lateral loading of a rigid rock socket embedded in a damage-susceptible poroelastic solid, International Journal of Geomechanics, 5: 276–285.

Souley M, Homand F, Pepa S, Hoxha D (2001) Damage-induced permeability changes in granite: a case example at the URL in Canada, Int J Rock Mech Min Sci 38: 297–310.

Tsang Chin-Fu, Bernier F, C. Davies (2005) Geohydromechanical processes in the Excavation Damaged Zone in crystalline rock, rock salt, and indurated and plastic clays—in the context of radioactive waste disposal. . Int J Rock Mech Min Sci 42:109–125.

Wang H.F (2000) Theory of linear poroeasticity, Princeton Univ. Press, 287p.

Table 1. Research teams and simulators applied in this study

Research Team	Numerical Simulator	Brief Description of Numerical Simulator and Model Approaches
CNSC: Canadian Nuclear Safety Commission	**FRACON**	The CNSC team used the basic THM formulation of Nguyen and Selvadorai (1995), originally implemented in the in-house FEM code FRACON, but for the analysis of the TSX experiment, the commercial general purpose FEM package COMSOL multiphysics was utilized. For the modeling of rock damage and permeability changes, the coupled THM formulation by Nguyen and Selvadurai (1995) was extended from linear elasticity to nonlinear elasto-plasticity. Damage was evaluated using the MSDPu criterion proposed by Aubertin and other (2000) and Li and others (2005).
JAEA: Japan Atomic Energy Agency's Research Team, including Hazama Cooperation	**THAMES**	THAMES is a finite-element code to simulate coupled THM behavior in a fully or partially saturated medium developed at Kyoto University, Japan (e.g., Ohnishi and others 1987, Kobayashi and others 2001). This code has been extensively applied in the DECOVALEX project and within the Japanese nuclear waste program (e.g., Rutqvist and others 2001b; Chijimatsu and others 2005). Along with the study presented in this report, a continuum-damage model was implemented. In this model the volumetric strain increases with damage evolution, resulting in changes in porosity that in turn are related to permeability of the medium.
CLAY-SKB: Clay Technology funded by the Swedish Nuclear Fuel and Waste Management Company	**ABAQUS**	The general-purpose commercial FEM code ABAQUS has been extensively applied by the Clay Technology for in the Swedish nuclear waste program as well in earlier DECOVALEX phases (e.g. Börgesson and others, 2001 Alonso and others 2005, Nguyen and others 2001). Damage around the TSX drift was considered using a modified Drucker-Prager plasticity model. Permeability change was not considered.
LBNL-SKI: Lawrence Berkeley National Laboratory funded by the Swedish Nuclear Power Inspectorate	**ROCMAS**	ROCMAS is a finite element program for analysis of coupled THM processes in porous and fractured rock developed at LBNL since the late 1980s (Noorishad and Tsang 1996; Rutqvist and others 2001a). The code has been extensively applied in earlier phases of the DECOVALEX project for THM analysis in bentonite-rock systems (e.g. Rutqvist and others 2005; Min and others 2005). In this study, a standard Mohr-Coulomb model was applied to simulate rock failure, and an empirical relationship between stress and permeability was used to simulate excavation-induced permeability changes.

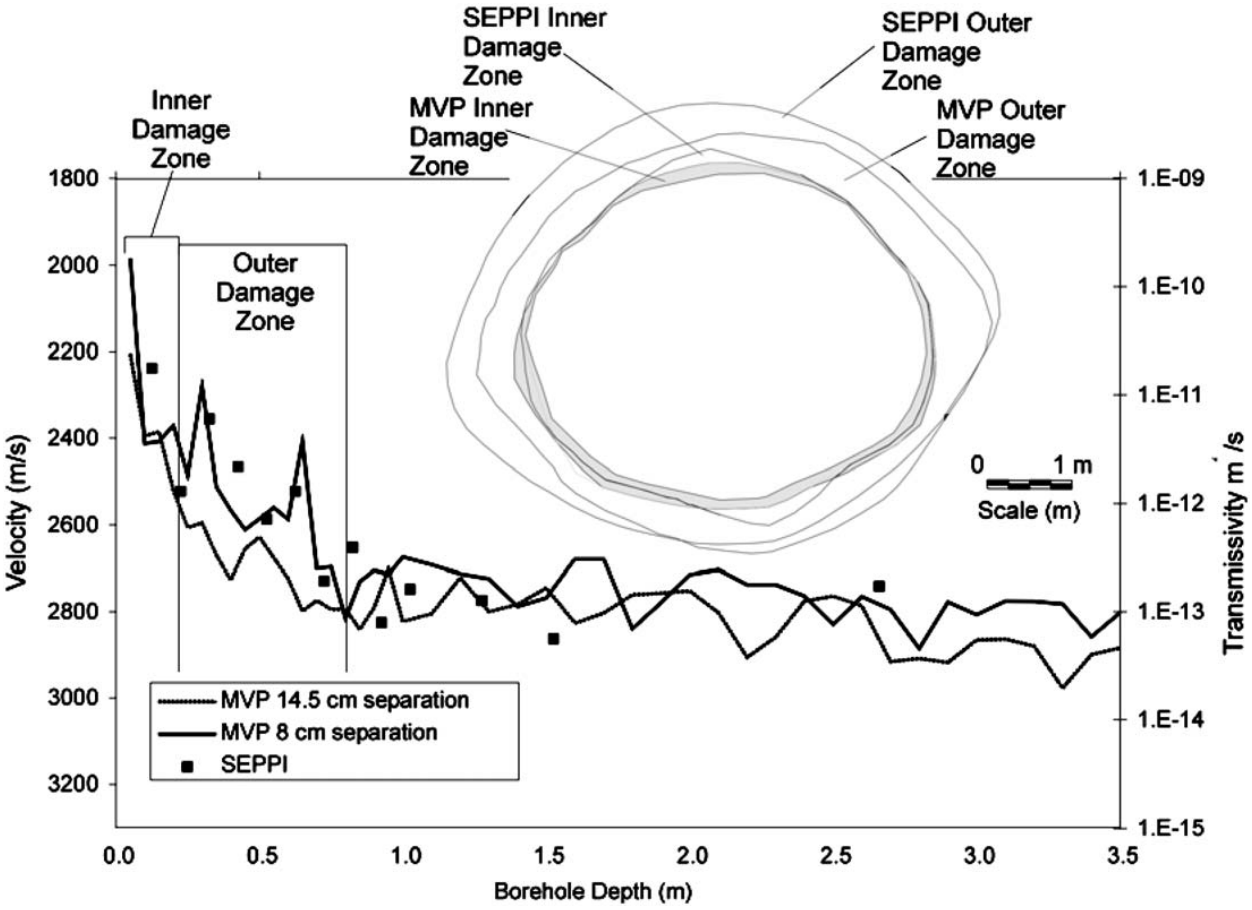

Figure 1. Change in velocity and hydraulic transmissivity indicating an inner and outer damage zone and the plot of inner and outer damage zone at the TSX tunnel, URL, Canada (Martino and Chandler 2004). MVP 14.5 cm and MVP 8 cm refers to MPV measurements using respectively 14.5 cm and 8 cm spacing between transmitter and receiver along the borehole.

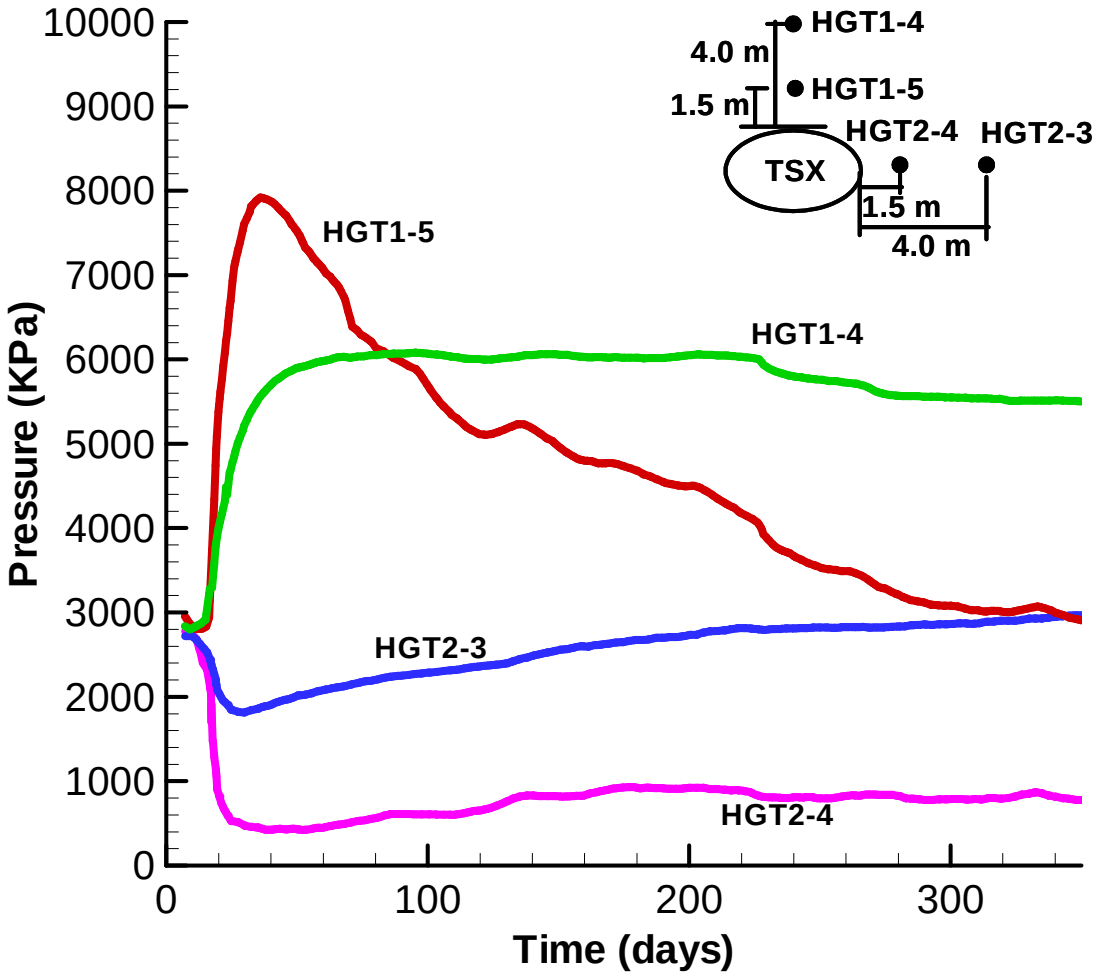

Figure 2. Pore pressure responses in the rock due to excavation of the TSX tunnel (data extracted from Chandler and others 2002).

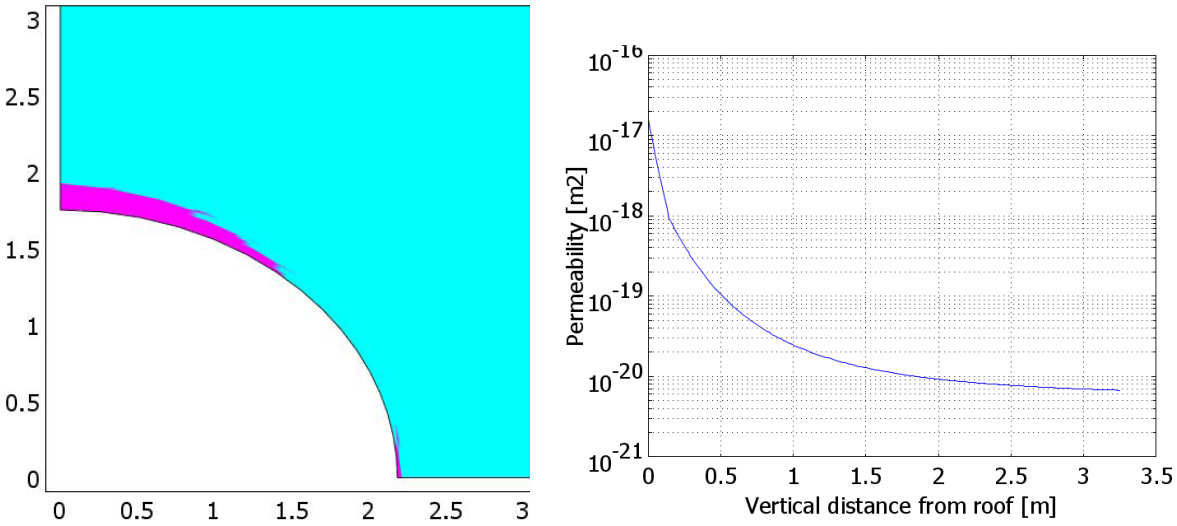

(a) (b)

Figure 3. The CNSC calculated (a) plastic zone (representing the inner damage zone) and (b) permeability changes along a profile extending upward from the top of the drift.

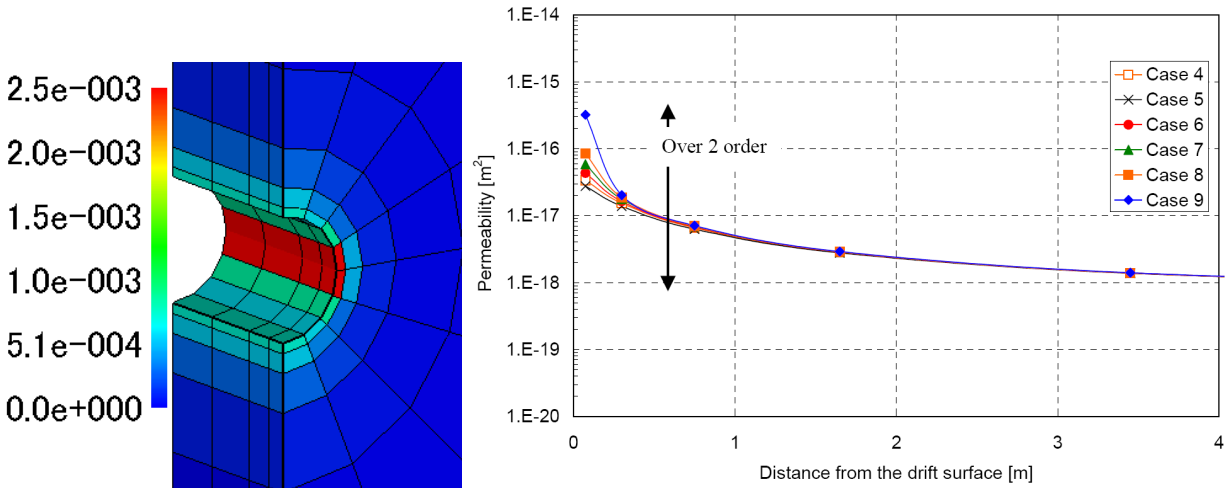

(a) (b)

Figure 4. The JAEA calculated (a) volumetric strain by damage and (b) permeability changes along a profile extending horizontally from the side of the drift. Case 4 to 9 in (b) represent different cases of lowering of the damage parameters B_0 and K_v with Case 9 representing the lowest values and best match to observed permeability change near the drift (Chijimatsu and others 2008b). The volumetric strain by damage shown in (a) is for Case 9.

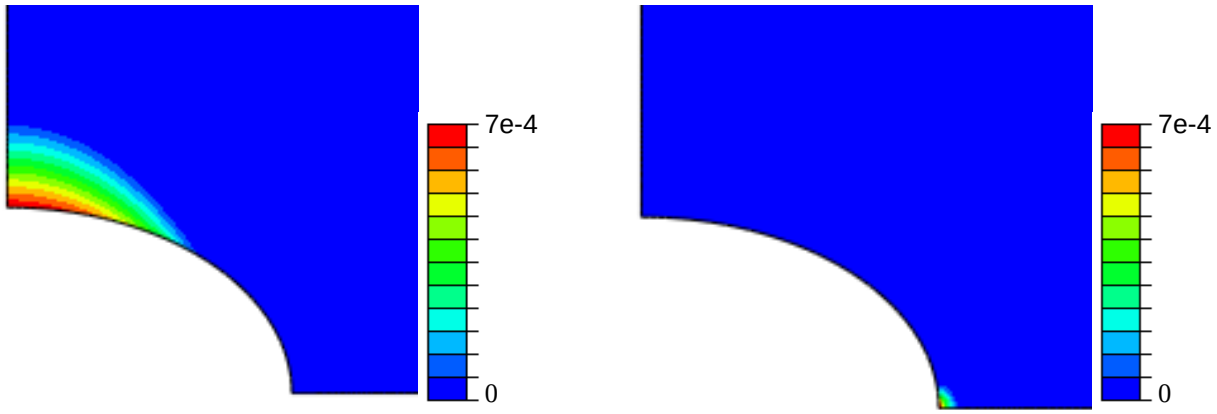

(a) (b)

Figure 5. The CLAY-SKB calculated equivalent plastic strain (a) for cohesion C = 60 MPa, and internal friction angle $\phi = 0$ and (b) for C = 0, and internal friction angle $\phi = 66°$ in the Drucker-Prager plasticity model.

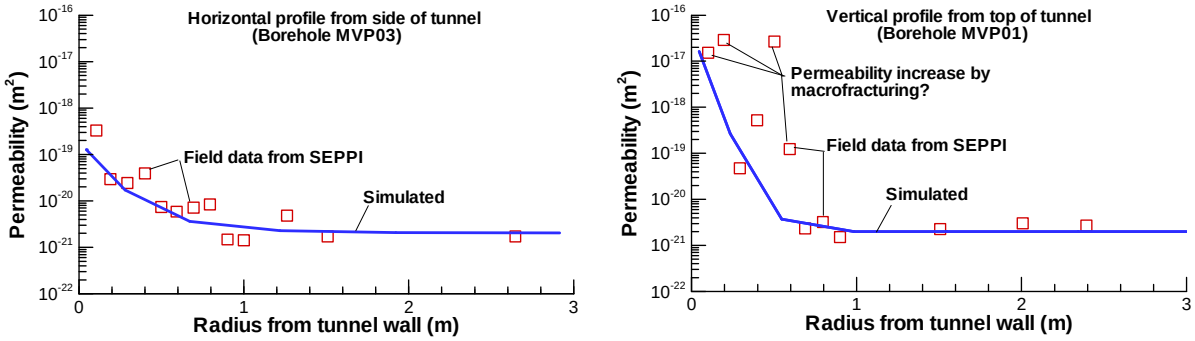

(a) (b)

Figure 6. Comparison of LBNL-SKI calculated and measured permeability profiles (a) extending horizontally from the side of the drift and (b) extending vertically from the top of the drift. The field data are SEPPI permeability extracted from Souley and others (2001).

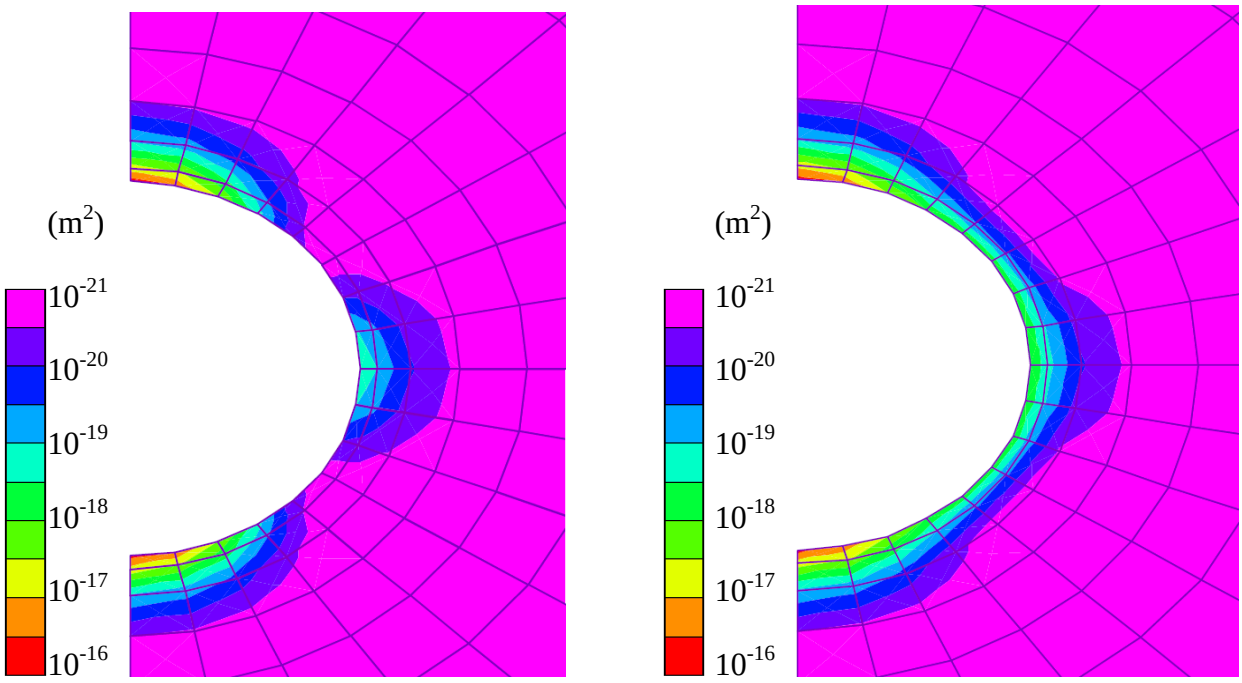

(a) (b)

Figure 7. LBNL-SKI calculated permeability distribution around the drift (a) without drill-and-blast-induced effects and (b) with effects of drill and blast added.

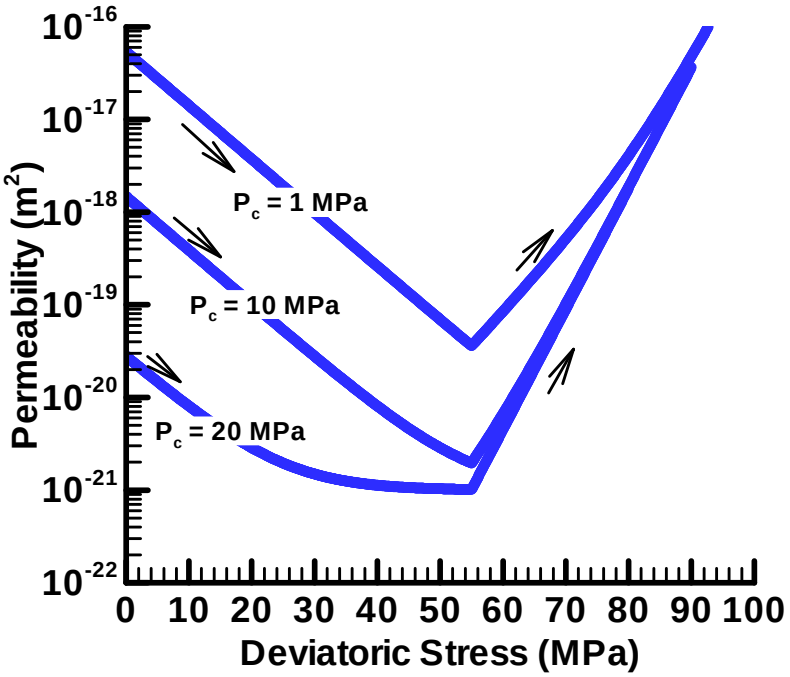

Figure 8. LBNL-SKI calibrated stress-versus-permeability relationship according to Equation (6), with $\beta_1 = 4 \cdot 10^{-7}$ Pa^{-1}, $k_r = 2 \cdot 10^{-21}$ m^2, $\Delta k_{max} = 8 \cdot 10^{-17}$ m^2, $\gamma = 3 \cdot 10^{-7}$ Pa^{-1}, and the critical deviatoric stress for onset of shear induced permeability set to 55 MPa.

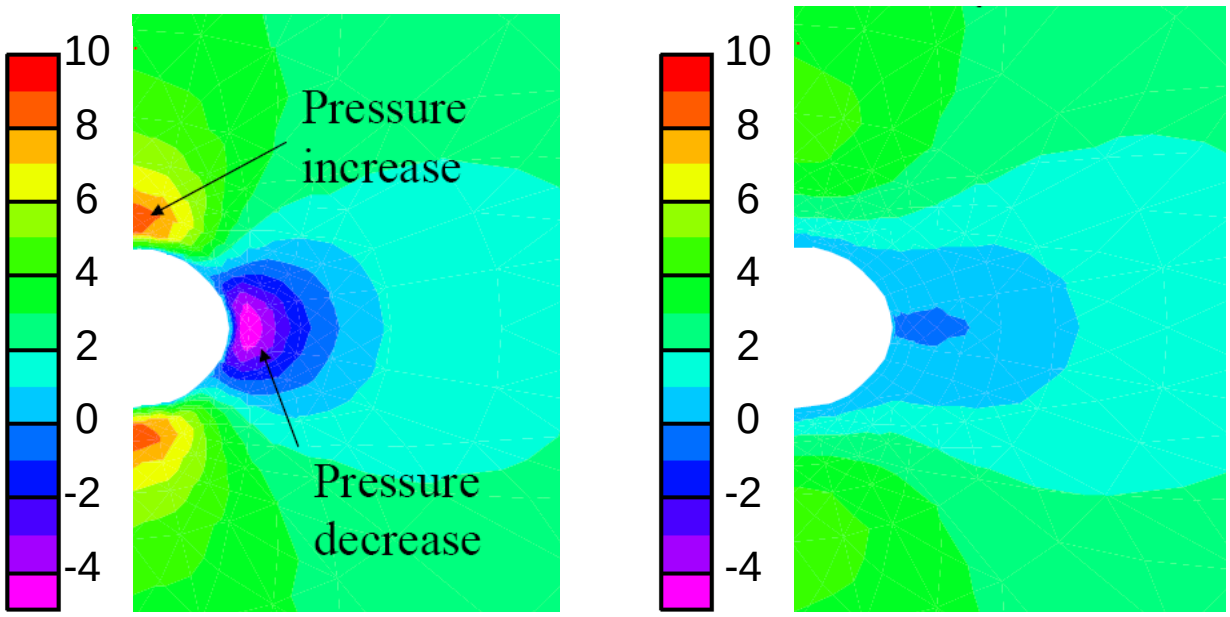

(a) (b)

Figure 9. Excavation induced pressure (in MPa) at (a) 1 months and (b) at 1 year (LBNL-SKI model).

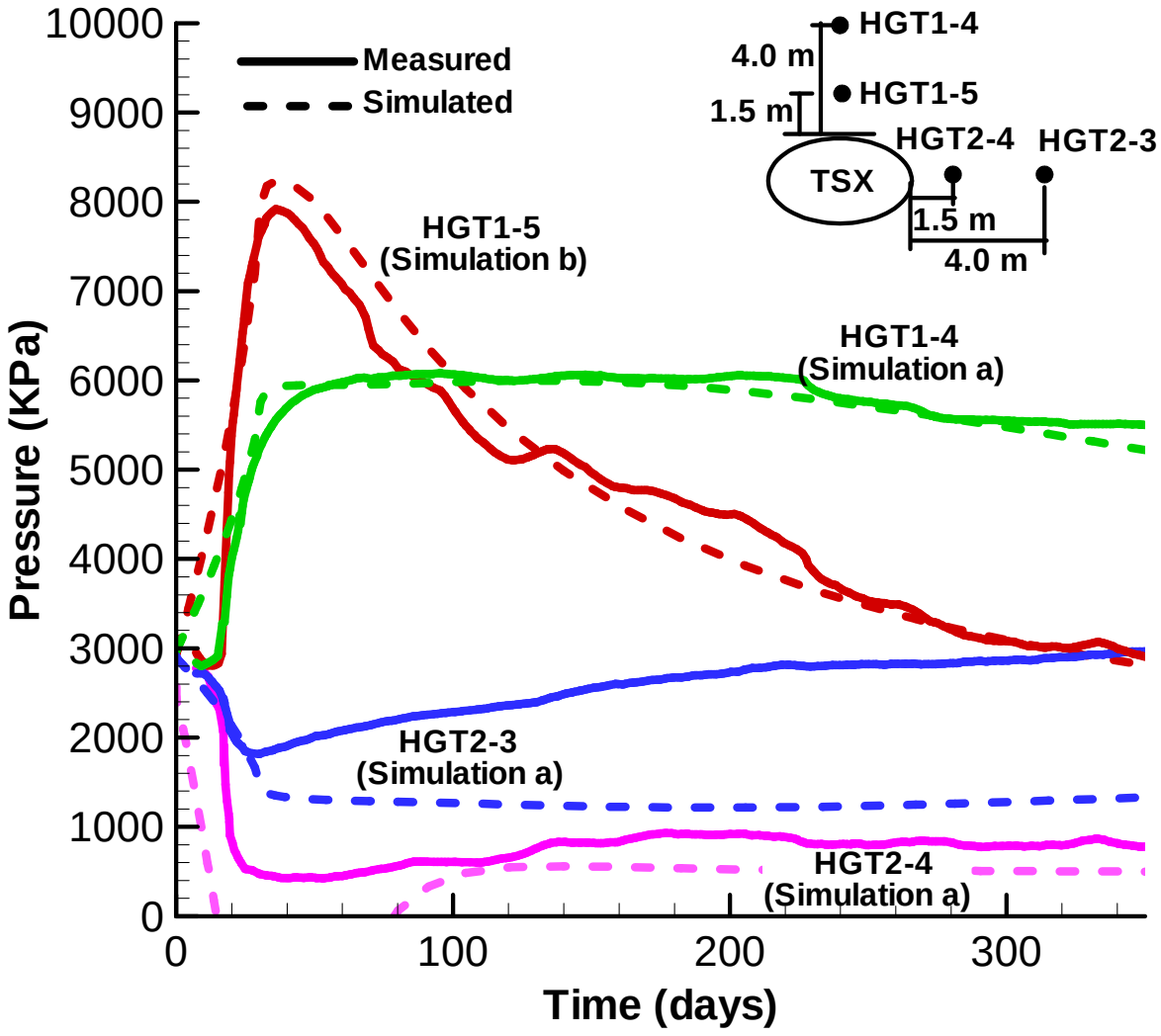

Figure 10. Comparison of calculated and measured pressure evolution (LBNL-SKI model).